Perspectives for Ag_2S NIR-II nanoparticles in biomedicine: from imaging to multifunctionality

Yingli Shen[1§], Jose Lifante[2§], Blanca del Rosal[3§], Erving Ximendes[4], Harrisson Santos[5], Diego Ruiz[6], Beatriz H. Juárez[6,], Jorge Rubio Retama[7], Emma Martín[8], Dirk Ortgies[4], Antonio Benayas[9,*] and Daniel Jaque[1,4,*].

[1]*Fluorescence Imaging Group, Departamento de Física de Materiales – Facultad de Ciencias, Universidad Autónoma de Madrid, C/ Francisco Tomás y Valiente 7, Madrid 28049, Spain*

[2]*Fluorescence Imaging Group, Departamento de Fisiología – Facultad de Medicina, Avda. Arzobispo Morcillo 2, Universidad Autónoma de Madrid, Madrid 28029, Spain*

[3]*Centre for Micro-Photonics, Faculty of Science Engineering and Technology, Swinburne University of Technology VIC 3122 Hawthorn, Australia*

[4]*Nanobiology Group, Instituto Ramón y Cajal de Investigación Sanitaria, IRYCIS, Ctra. Colmenar km. 9.100, Madrid 28034, Spain*

[5]*Grupo de Nano-Fotônica e Imagens, Instituto de Física, Universidade Federal de Alagoas, Maceió-AL 57072-900, Brazil*

[6]*IMDEA Nanoscience, Faraday 9, Campus de Cantoblanco, Madrid, Spain*

[7]*Department of Applied Physical Chemistry and Condensed Matter Physics Center (IFIMAC), Universidad Autónoma de Madrid, 28049 Madrid, Spain*

[7]*Departamento de Química en Ciencias Farmacéuticas, Facultad de Farmacia, Plaza de Ramón y Cajal, s/n, Universidad Complutense de Madrid, Madrid 28040, Spain*

[8]*Fluorescence Imaging Group, Departamento de Física Aplicada – Facultad de Ciencias, Universidad Autonoma de Madrid, C/ Francisco Tomás y Valiente 7, Madrid 28049, Spain*

Department of Physics and CICECO—Aveiro Institute of Materials University of Aveiro 3810-193 Aveiro, Portugal

§: Authors contributed equally

Corresponding authors: abenayas@ua.pt and daniel.jaque@uam.es

Abstract:

Research into near infrared (NIR) bioimaging has progressed very fast in the past few years, as fluorescence imaging is reaching a credible implementation as preclinical technique. The applications of NIR bioimaging in theranostics have contributed to its increasing impact. This has brought about the development of novel technologies and, simultaneously, of new contrast agents capable of acting as efficient NIR optical probes. Among these probes, Ag_2S nanoparticles (NPs) have attracted increasing due to their temperature-sensitive NIR-II emission, which can be exploited for deep-tissue imaging and thermometry, and their heat delivery capabilities. This multifunctionality makes Ag_2S NPs ideal candidates for theranostics. This review presents a critical analysis of the synthesis routes, properties and optical features of Ag_2S nanoparticles. We also discuss the latest and most remarkable achievements enabled by these NPs in preclinical imaging and theranostics, together with a critical assessment of their potential to face forthcoming challenges in biomedicine.

I.- Introduction.

Fluorescence bioimaging emerged in the last decade as a promising complementary technique to other imaging modalities such as computerized tomography, (CT) or magnetic resonance imaging (MRI). The advantages of fluorescence imaging over these well-established techniques are: (i) the use or non-ionizing radiation as excitation source; (ii) the possibility of real-time imaging thanks to a fast scanning speed plus the edge of not requiring data post-processing; (iii) its experimental simplicity, which makes it a cost-effective technique. Fluorescence imaging is a well-established technique for cell and tissue imaging (*in vitro*). Organic fluorescent labels, including dyes and fluorescent proteins, are the most commonly used contrast agents in this case.[1] These labels present fluorescence bands in the visible spectral range under ultraviolet/visible optical excitation, which enables three-dimensional intracellular imaging thanks to the reduced thickness and high transparency to visible radiation of the cell samples. The poor stability of these labels, however, motivated the search of alternatives for fluorescence imaging. This resulted in the development of luminescent nanoparticles (NPs).

In the 90s, semiconductor NPs, particularly quantum dots (QDs), became widely used contrast agents for *in vitro* fluorescence imaging.[2] Semiconductor NPs present outstanding optical properties that include a high photochemical stability, large absorption cross sections, high fluorescence quantum yields, easy surface decoration and the possibility of tailoring their optical properties mainly according to composition and size.[3, 4] This made semiconductor NPs the most popular inorganic fluorescent labels for cellular imaging ahead of other competing systems, including upconversion NPs, organic NPs and metallic NPs. Semiconductor NPs also allow two-photon imaging and contactless temperature sensing *via* luminescence thermometry, greatly increasing the interest on these materials.[5-7]

The first imaging experiments in small animal models using QDs as contrast agents revealed their great potential as fluorescent labels for in vivo research.[8, 9] However, only images with a limited penetration could be built from their fluorescence. The limiting factor was the strong attenuation of visible light by tissues, which effectively reduces the optical penetration of visible-emitting QD-based images down to few millimeters.[10-12] High penetration *in vivo* imaging requires contrast agents working in the biological windows, spectral ranges where tissues becomes partially transparent.[11, 13]

Recent works have demonstrated the convenience of using fluorescent probes optically excited in the first biological window (NIR-I, 700-950 nm) that show fluorescence bands in the second biological window (NIR-II, 1000-1700 nm).[13] There are numerous examples of semiconductor NPs satisfying these conditions including, as one of the most representative examples, PbS semiconductor NPs. Adequate surface coating of PbS QDs allows the acquisition of high contrast, high penetration, *in vivo* images by using ultra low illumination intensities and administration doses.[14-16] Despite their adequate optical features, the clinical potential of PbS QDs is limited due to the presence of heavy metals, which raises concerns about long-term accumulation and toxicity. Developing heavy metal-free NIR-II contrast agents is essential for the translation of NIR-II *in vivo* imaging

into the clinics. There are few semiconductor NPs that fulfill these requirements. Among them, Ag_2S NPs are the most well-researched system with demonstrated applications in preclinical research.

In this article, we provide a critical summary of the fundamental properties of Ag_2S NPs and highlight the most recent advances for preclinical applications. This review is structured in five sections. In **Section II**, we discuss the different synthesis routes used for the fabrication of Ag_2S NPs and their impact on their optical properties. **Section III** describes the optical properties of Ag_2S nanoparticles that allows their use as multifunctional probes. **Section IV** summarizes the most recent advances in the application of Ag_2S nanoparticles for *in vivo* biomedical research. Finally, in **Section V** we discuss the limitations that could prevent the clinical translation of Ag_2S NPs, the challenges that need to be faced in the near future, and the novel forthcoming applications of Ag_2S NPs in nanomedicine.

II.- Impact of synthesis routes on the optical properties of Ag_2S nanoparticles.

Ag_2S is one of the most interesting sulphide materials due to its composition, material structure and optical features explained below. It can be found in three different crystal structures, which depend on the temperature: monoclinic α-Ag_2S, (stable up to 178 °C), body-centered cubic Ag_2S (stable from 178 to 600 °C) and face-centered cubic γ-Ag_2S (stable above 600 °C). The monoclinic bulk α-Ag_2S is one of the oldest known semiconductor materials, which can be traced back to 1833, when Michael Faraday discovered the capacity of bulk Ag_2S to behave as insulator at room temperature and to be highly conductive at elevated temperatures.[17] Today, it is well known that α-Ag_2S is a semiconductor material, showing a direct and narrow band gap at room temperature (E_g = 1 eV), with a relatively high absorption coefficient for wavelengths shorter than 850 nm.[18] In addition, α-Ag_2S exhibits good chemical stability and excellent optical properties when compared with other reference systems such as fullerene or chloroaluminium phtalocyanine. The emission of bulk Ag_2S is centered at around 1200 nm corresponding to an electron de-excitation via exciton recombination. The electronic transition from the valence band to the conduction band is essentially a charge transfer from 3p (S) to 5s (Ag) orbitals.[19]

The chemistry of Ag_2S can be described as relatively simple, and the synthesis of Ag_2S NPs can be catalogued as straightforward when compared to the synthetic routes required for the fabrication of other infrared-emitting nanostructures such as single-walled carbon nanotubes (SWNTs) or lanthanide-doped dielectric NPs (Ln-NPs).[20, 21] However, obtaining a highly efficient Ag_2S matrix is challenging due to the high mobility of Ag ions, which exhibit an activation energy barrier of 0.425-0.477 eV.[22] In addition, the high reactivity of the

Ag ions under regular synthetic conditions favors the formation of metallic Ag phase within the Ag_2S matrix, which provoke cation deficiencies, crystal defects and midgap states. All of them together may be responsible for the low quantum yield (QY) of the majority of the reported Ag_2S NPs.[23] For this reason, seeking a technique to effectively reduce this intrinsic drawbacks of Ag_2S is essential in order to produce high-quality Ag_2S NPs and improve their optical performance.

Ag_2S NPs have been synthesized using different methods. Some representative examples are:

i) Solid-phase conversion of Ag NPs in polymer or zeolites supports.[24, 25]

ii) Co-precipitation reaction between Ag^+ ions and S^{2-} in the presence of a stabilizing agent such as thiols or polymers.[26, 27] The ultra-low solubility product of Ag_2S ($K_{sp} = 6.1 \cdot 10^{-51}$) makes the nucleation of Ag_2S thermodynamically hard to control, even at lower temperature, complicating size control and dispersion of the NPs.

iii) Synthesis in polar media in the presence of albumin. This method has been successfully applied to the synthesis of NPs with sizes ranging between 1.6 and 7 nm.[28]

iv) Thermal decomposition in organic media at high temperature, which has become the most used route to produce monodisperse and size controlled NPs.[29]

Due to the existence of such diversity of synthesis routes, it is possible to find in the literature numerous works reporting on the synthesis of Ag_2S NPs with sizes ranging from 1.5to 10 nm. These works report on very different optical properties for the Ag_2S NPs. In order to stablish a correlation between the particle size and their emission properties we have represented in **Figure 1a** the central emission wavelength of Ag_2S nanocrystals as a function of their size. Data have been obtained from the analysis of **References 30-57**. Strong variations of the emission peak position are observed for Ag_2S NCs with sizes below ~4 nm. In contrast, Ag_2S NPs with sizes above 4 nm present emission peaks localized between 1050 and 1250 nm (±0.2 eV) in most reports. The here performed analysis of the published data can be well-explained considering a Bohr exciton radius for Ag_2S close to 2 nm. The fluorescence of nanoparticles smaller than 4 nm are, therefore, affected by quantum confinement effects that results in a blue-shift of emission with the decreasing size. On the other hand, Ag_2S nanocrystals with diameter larger than 4 nm behave as “bulk” units and their fluorescence wavelength is purely given by the intrinsic band-gap of Ag_2S. This conclusion is,

indeed, in accordance with previous experimental works focused on the determination of the Bohr radius of Ag_2S.[30]

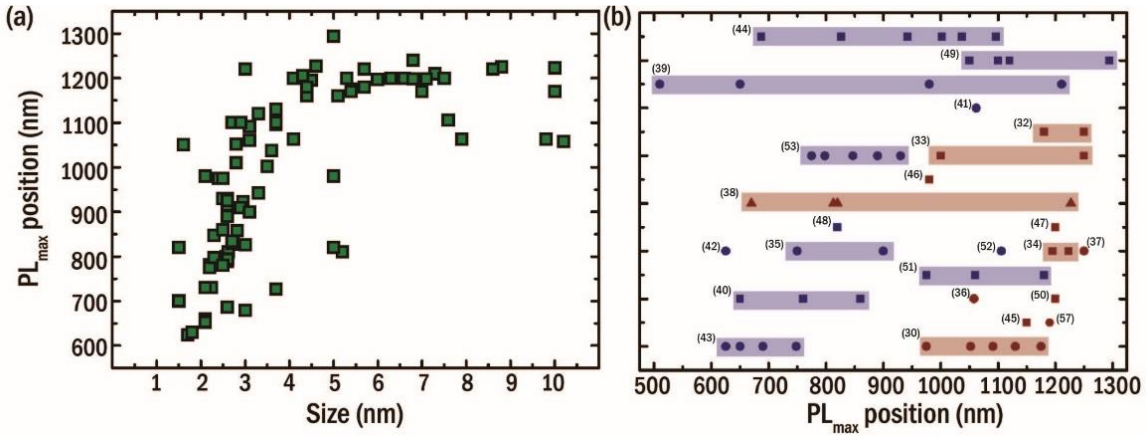

Figure 1. a) Comparison of the PL maxima of Ag_2S NCs with their size as reported in references [30-57] **b)** Spectral position of the PL maximum depending on the synthetic approach (■ for hot injection, ●- for heat-up and ▲- for seeded growth) and the polarity of the media (organic in red and polar in blue). Color bands are used for NCs in the same report. Data extracted from references [30, 32-34, 36-52, 57]

It is worth mentioning, however, that the synthetic route seems to play a critical role in the optical properties of Ag_2S NPs. Ag_2S NPs produced by synthetic routes based on the decomposition of metallic salts in organic media (normally in the presence of 1-dodecanethiol) show emission bands in the NIR-I or NIR-II ranges (800-950 and 1000-1500 nm, respectively) and limited size tunability. In contrast, most of the synthesis routes carried out in polar media (water, ethylene glycol) yield Ag_2S NPs with blue-shifted emission bands in the VIS range (500-800 nm), and higher size tunability. This is exemplified in the selected examples shown in **Figure 1b**, where blue and red lines correspond to syntheses carried out in polar and organic media, respectively. The dots embedded, squares and triangles in the different line correspond to the central emission wavelengths of different NP sizes.

III.- Optical properties of Ag_2S nanoparticles: An unique multifunctional system.

Ag_2S NPs larger than 4 nm in diameter present an emission band centered at around 1200 nm (see Fig. 1). This NIR-II emission is not a unique feature of these NPs, as other systems also present strong emission in this wavelength range, other semiconductor NPs, SWNTs, rare-earth-doped NPs or dyes.[58-62] What makes Ag_2S NPs unique is the strong temperature dependence of their emission in the relevant temperature range for biological applications (around 37 ºC). This enables the use of Ag_2S NPs not only as NIR-II contrast agents but also as *in vivo* fluorescent nanothermometers.[63-67] **Figure 2a** shows the emission spectra as obtained from a colloidal dispersion of Ag_2S NPs (10 nm in diameter) obtained

under continuous wave excitation at 808 nm for temperatures ranging between 24 ^{o}C and 60 ^{o}C. The most noticeable effect is the strong fluorescence quenching that happens in this relatively narrow temperature range (see **Figure 2b** for the temperature dependence of the integrated emission intensity). Note that the 1200 nm fluorescence band is quenched by almost 90 % for an absolute temperature change as small as 18 % (90 % quenching is produced for an absolute temperature increment from 293 up to 333 K). Although in previous works the relationship between fluorescence intensity and temperature has been postulated to be linear,[54] this is only true for temperatures below 45 ºC. The nonlinear thermal quenching of Ag_2S NPs has never been discussed in detail but, for applications using their intensity as an indicator of local temperature, the knowledge about the exact origin of this thermal quenching is essential. It should be noted that this relevant thermal quenching is also evidenced in the temperature dependence of the Ag_2S fluorescence lifetime.[68] **Figure 2c** shows the fluorescence decay curves of PEG-coated Ag_2S dispersed in water at two different temperatures. A clear reduction in the fluorescence decay time is observed for higher temperatures, as seen in **Figure 2d**, where the temperature dependence of the fluorescence lifetime of these NPs is shown. Close to room temperature, the fluorescence decay time decreases at a rate as large as 4%·ºC^{-1}. This is more than twice the decrease rate reported for semiconductor NPs emitting in the visible and highlights the potential use of Ag_2S NPs for lifetime-based luminescence nanothermometry.[68] Nevertheless, practical implementation of this technique is not easy, as short pulse lasers and fast detectors are required for excitation and emission, respectively. From a practical standpoint, this is harder for *in vivo* measurements but not at the *in vitro* level, where the basic principles available for lifetime microscopy can be applied.[69] The analysis of the fluorescence decay curves also provides fundamental information about the physics behind the luminescence properties of Ag_2S NPs. In particular, the nonexponential character of the decay curves has been attributed to the interplay between bulk and surface de-excitations that are ultimately related to the presence of surface defects.[68] Thus, the presence of quenching defects can be monitored by analysing the fluorescence decay curves of Ag_2S NPs, in turn providing feedback to improve the synthesis routes towards brighter Ag_2S NPs.

Temperature increases also cause a significant redshift in the emission of Ag_2S NPs, as shown in **Figure 2e.**The thermal spectral shift of semiconductor NPs has been extensively studied and constitutes the basis of semiconductor NP-based luminescence nanothermometry.[7] In most systems (for instance, CdTe or CdSe), the thermal spectral shift coefficient is determined by the temperature dependence of different physical parameters: energy gap, electron-phonon coupling, quantum confinement and lattice parameter.[70] This multiparametric dependence makes it difficult to elucidate a priori the temperature dependence of the emission wavelength and, hence, its use as a robust parameter for thermal sensing. For large (> 4 nm) Ag_2S NPs, the redshift of the emission peak follows

a linear trend with temperature at a rate of -1.08 eV/ºC. This is very similar to the thermal shift rate previously reported for bulk Ag_2S (-1.1. eV/ºC), indicating that the thermal spectral shift of large Ag_2S nanocrystals is mainly given by the temperature dependence of the Ag_2S energy gap.[71] This was expected due to the absence of quantum confinement effects, as discussed previously. From a practical point of view, this also allows establishing an unequivocal relation between emission peak and local temperature by just applying a simple linear relationship. This suggests that Ag_2S NPs would behave as primary nanothermometers (capable of providing contactless absolute temperature readouts) based on a simple spectral analysis of their emission band.[72, 73] Nevertheless, this has not been demonstrated yet.

The temperature-induced spectral shift also changes the relative emitted intensity at two different wavelengths, allowing ratiometric temperature sensing. As an example, **Figure 2f** shows the temperature dependence of the ratio between the intensities emitted at 1161 nm and 1249 nm. As a direct consequence of the already described spectral redshift, this intensity ratio increases with temperature at a rate of 3 %·ºC^{-1}. This is significantly higher than the temperature-induced intensity ratio change reported for other NIR-II emitting ratiometric nanothermometers (below 1%·ºC^{-1} for neodymium-doped NPs).[74, 75] Thus, Ag_2S NPs stand out as highly sensitive ratiometric temperature sensors, unaffected affected by local variations of Ag_2S NPs and capable –in principle- of providing an absolute temperature readout. Despite not requiring complex experimental setups, Ag_2S NPs have not been applied yet for ratiometric temperature sensing *in vivo*.

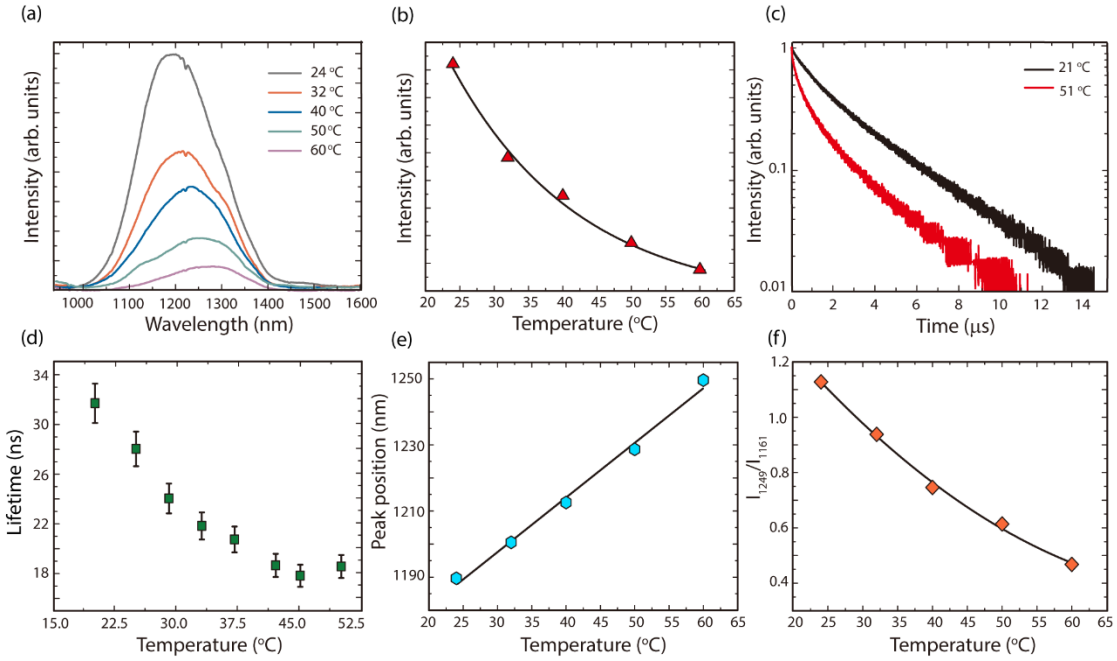

Figure 2. (a) Emission spectra of Ag_2S NPs (10 nm in diameter) for temperatures between 24 ºC and 60 ºC. **(b)** Temperature dependence of the 1200 nm emission intensity generated by Ag_2S NPs. **(c)** Fluorescence decay curves of Ag_2S NPs dispersed in water at two different temperatures. **(d)** Temperature dependence of the fluorescence lifetime of Ag_2S NPs in water. **(e)** Ag_2S NPs emission peak position as obtained for different temperatures (dots are the original data and solid is the best linear fit). **(f)** Temperature dependence of the ratio between the emitted intensities at 1161 nm and 1249 nm. Dots are experimental data and solid line is just a guide for the eyes.

Ag_2S NPs typically show relatively low fluorescence QYs. It is possible to find in the literature numerous works reporting on QYs as large as 10% for Ag_2S NPs.[57, 76] In most cases, these values were obtained doing comparative studies using infrared-emitting dyes as a reference. However, the QY of commercial PEG-coated, water-dispersed Ag_2S NPs measured using an integrating sphere (absolute determination of QY) is below 1%.[32] Such a low QY is consistent with the short fluorescence decay times, indicating a large non-radiative de-excitation probability.[68]

Typically, low QYs are considered a drawback when dealing with fluorescent probes as they limit their overall brightness. Nevertheless, the brightness of Ag_2S NPs allows deep-tissue in vivo imaging possible, as has been widely demonstrated. The low QY adds an extra functionality to these NPs, as it leads to a leads to a photothermal conversion efficiency (fraction of absorbed optical power that is converted into heat) above 99%. Thus, Ag_2S emerges as a unique system that simultaneously features the trifecta of capabilities for *in vivo* imaging, *in vivo* thermal sensing and remote heating. This possibility, already demonstrated with PbS QDs, upconverting NPs, and neodymium NPs remains unexplored with Ag_2S NPs.[74, 77, 78] remains unexplored with Ag_2S NPs.

As a summary, **Table I** includes a comparison of the characteristics of different NIR-II luminescent probes including Ag_2S NPs and their NIR-II emitting competitors in the roles of contrast agents, nanothermometers or light-activated heating sources. It is evident from **Table I** that Ag_2S NPs emerge as the most promising multifunctional NIR-II nanostructures.

System	NIR-II Brightness	Thermal sensitivity	Synthesis simplicity	Heating efficiency
Ag_2S		□	□	□
CNTs	□	□	□	□
Ln^{3+}:NPs	□	□	□	□
ICG	□	□	□	□

□ = *Excellent* □= *Good* □= *Fair* □= *Mediocre* □ = *Bad*

Table I.- Schematic comparison of the multifunctional character of NIR-II emitting systems used for in vivo imaging. CNTS: carbon nanotubes; Ln^{3+}; NPs: lanthanide-doped nanoparticles; ICG: indocyanine green (dye).

IV.- Recent advances in bioimaging and biosensing based on Ag_2S NPs.

IV.a.- Ag_2S NPs for in vivo diagnosis based on transient thermometry.

As discussed in **Section III**, Ag_2S NPs are one of the very few NIR-II luminescent probes capable of simultaneous heating and remote thermal sensing under single beam optical excitation. Their heavy-metal-free composition and their high multiparametric thermal sensitivity put Ag_2S NPs ahead of the only other available NIR-II thermometer/heater system (PbS QDs). In the past, a small group ofsystems with this multifunctional character have enabled *in vivo* tumor treatment via fully controlled photothermal therapy.[74, 77, 78] Though a similar approach could be used with Ag_2S NPs, this possibility remains unexplored.

In spite of this, Ag_2S NPs have played a leading role in the recent development of transient thermometry (TTh) as a diagnosis tool. The TTh technique relies on the dependence of the conduction of heat inside a perfused tissue on various biophysical properties (tissue density, specific heat and thermal conductivity; metabolic generation; blood perfusion rate and core body temperature) which may be altered by developing diseases. This is reflected in Pennes bioheat model, which is usually employed to describe *in vivo* thermal dynamics.[79-81] TTh is based on the analysis of the thermal relaxation curve of tissues, that is, the time evolution of their temperature after being subjected to a heating pulse until they return to baseline temperature. (**Figure 3a**). This has been demonstrated in vivo for subcutaneous tissue in healthy mice using different NIR-II-emitting NPs.[64, 82] However, the thermal relaxation profile can provide information about the health status of the tissue under study, as demonstrated with PbS QDs in a mouse model of ischemia. The results showed a marked difference between the thermal relaxation times of ischemic and healthy tissues. [83]

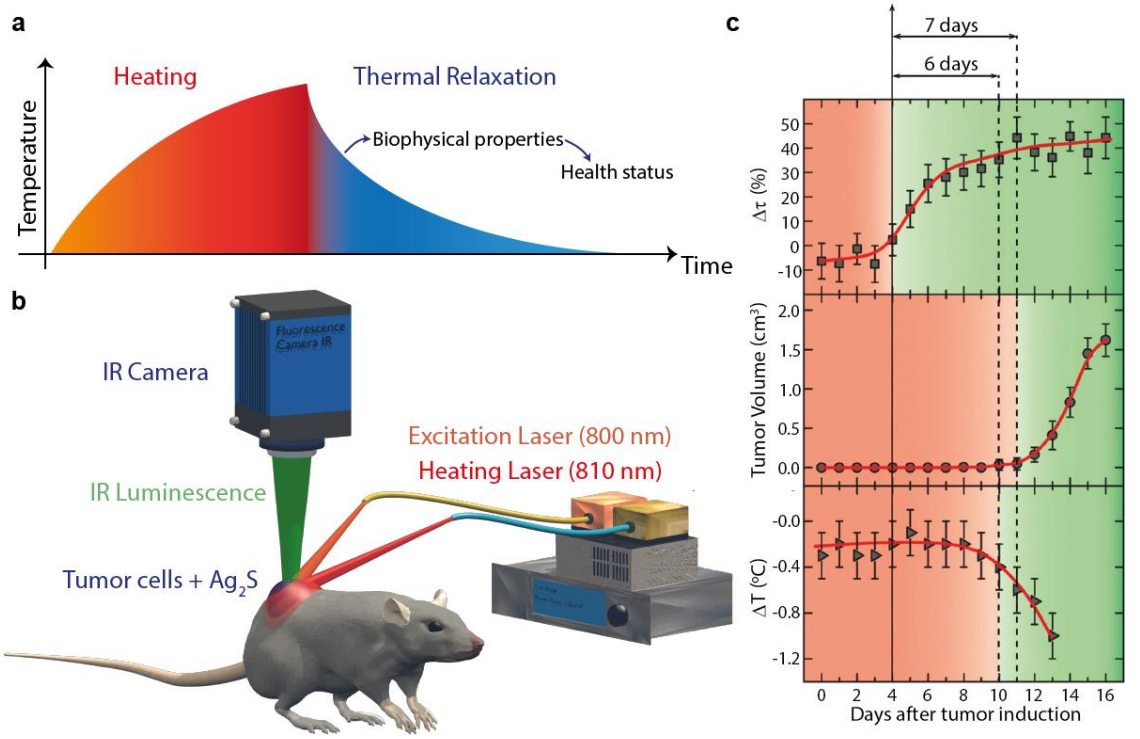

Figure 3. **a)** Schematic representation of the working principle of transient thermometry (TTh). **b)** Schematic diagram of the experimental setup used for *in vivo* measurement of thermal transients in both tumoral and healthy tissues. The use of two infrared lasers is illustrated, as well as the presence of Ag_2S nanothermometers. **c)** Time evolution of Δτ, tumoral volume and surface temperature difference between tumor and healthy tissue. The background colors and vertical lines indicate the time when the tumor becomes detectable by the different methods. Adapted with permission from reference 83. Copyright 2018, Wiley- VCH.

Recently, this technique has been used to evaluate impact of tumor development on tissue thermal dynamics in a murine model of melanoma using Ag_2S NPs. [84] The NPs were injected intratumorally to ensure deep tissue temperature sensing at the tumor site. The evolution of the thermal dynamics was studied throughout its development from induction (day 0) until necrosis became visually evident (around day 14), while keeping track of its size and surface temperature. The experimental setup used is schematically shown in **Figure 3b**. An 810 nm heating laser was used to elicit a moderate temperature increase (<7 °C) at the tumor site and was switched off after 4 min. A second laser (800 nm), operating at a reduced intensity, achieved optical excitation of the Ag_2S and was kept on throughout the experiment. The potential use of TTh as a tumor early diagnosis tool was evidenced by the data included in **Figure 3c.** It shows the time evolution (measured since the day of tumor induction) of Δτ (normalized difference between the thermal relaxation time of tumoral tissue with respect to that of the healthy tissue), tumor size and of the surface temperature difference between tumoral and healthy tissues, as measured by infrared thermography. Results concluded that TTh significantly shortened the time required for tumor detection by 60% when compared with the traditional diagnosis based on optical inspection or

infrared thermography. This change in the thermal dynamics was correlated with changes in the thermoregulation mechanisms through changes in the blood perfusion, as well as with changes in the metabolic heat generation during tumor development, specifically during the transition between angiogenesis and necrosis.

Though Ag_2S-based TTh is just in its first steps, it is reasonable to think that in the long-runAg_2S NPs will enable the study of complex heat transfer mechanisms in biological systems.

IV.b.- Ag_2S NPs for brain studies.

Fluorescent NPs have arisen as potential theranostic tools with reduced cost and high temporal and spatial *in vivo* resolution in the field of brain research, with a wide range of applications including specific drug targeted delivery, controlled photothermal therapy or imaging studies. Targeting NPs for brain applications is particularly challenging due to the existence of the blood-brain barrier (BBB), the physical barrier that intimately separates and controls the traffic of molecules into the brain parenchyma. Several strategies have been explored for successful delivery of NPs to the brain, such as the selection of specific administration routes, BBB transient artificial breakdown or NP functionalization with peptides that target specific receptors expressed in the cells comprising the BBB.[85]

Different NPs, including carbon nanotubes, polymeric NPs and IR dye-loaded liposomes, were applied in brain research. A detailed description of the different NPs used for brain studies can be found in a recent review article by Wang *et al*.[86] The number of studies relying on NIR-II Ag_2S fluorescent nanoprobes for brain applications is strikingly limited, and thus, the potential applicability of Ag_2S QDs as theranostic agents remains mostly unexplored.

Li C. *et al.* designed a dual-modality Gd-DOTA-Ag_2S QDs nanoprobe combining the deep tissue penetration of enhanced magnetic resonance imaging (MRI) of Gd with the high-signal-to noise ratio and high spatiotemporal resolution of the NIR-II fluorescence of Ag_2S QDs.[87] The authors used a mouse model of induced brain tumor employing U87MG injected cells to ascertain the potential of this system as a dual tool that allows the preoperative tumor detection and intraoperative tumor visualization in order to increase the precision during tumor resection. The NIR-II fluorescence imaging of Ag_2S QDs allowed precise intraoperative resection of the tumor as shown in **Figure 4a** and **4b**. NIR-II-guided surgery resulted in a 3-fold reduction in the number of residual tumoral cells compared to those present after naked eye surgery. The Gd-DOTA-Ag_2S QDs showed no remarkable *in vivo* toxicity for up to 1 month after administration. Thus, Ag_2S-based nanoprobes arises as a novel tool that could improve the detection and operation strategy in future clinical applications in different contexts such as brain cancer resection, in which a high precision is essential to achieve a complete tumor resection.

To the best of our knowledge, the only other work employing Ag_2S nanoprobes for brain studies relied on their robustness as nanothermometers. Variations in brain temperature are typically small (< 3°C) due to the presence of regulatory mechanisms based in the interplay between cerebral blood flow and cerebrospinal fluid circulation.[88-93] These mechanisms maintain brain temperature within a narrow range, making high thermal sensitivity an essential feature of any luminescent nanothermometers applied for recording brain temperature. Ag_2S NPs, with their thermal sensitivity of up to 4 %/°C, allow recording sub-degree temperature changes. Our group recently applied them to detect brain temperature in living mice intracerebral injected with Ag_2S NPs.[94] The analysis of the NIR-II fluorescence emitted by the intracranial Ag_2S NPs under 808 nm optical excitation (**Figure 4d**) provided a remote (contactless) reading of the brain temperature. The possibility of extracting the brain temperature from a straightforward analysis of the fluorescence intensity generated by the intracerebral allocated Ag_2S NPs was first demonstrated by monitoring a mouse subjected to a moderate (< 7 °C at the skin surface) laser-induced heating. The normalized temperature versus time curves measured at the skin and the brain displayed identical trends, indicating the unequivocal relationship between the emission of injected Ag_2S NPs and brain temperature. Ag_2S nanothermometers also allowed us to provide further evidence supporting the existence of mechanisms that regulate brain temperature. During a whole-body cooling process, the core temperature of an anesthetized CD1 mouse fell down to 18 °C (almost 20 °C from its baseline temperature), while the brain temperature only deviated by 3 °C from its baseline value and showed a three-fold slower rate of change. In a mouse model of barbiturate coma (induced by a sodium pentobarbital injection), Ag_2S NPs enabled obtaining experimental evidence on the strong link between brain temperature and activity. As seen in **Figure 4f**, the time evolution of the brain temperature extracted from the NIR- II emission intensity of intracerebrally injected Ag_2S NPs, indicated that the pentobarbital injection produced a slight (close to 1 °C) decrease in brain temperature, while no skin cooling occurred (**Figure 4f**). This indicated the direct association of the drop in brain temperature with barbiturate- induced decrease in brain metabolic activity and evidenced the capability of Ag_2S nanoparticles to measure small temperature changes, as is essential for brain thermometry.

As has been discussed in this section, Ag_2S nanoprobes have great potential for application in brain studies despite the limited research carried out in this area so far.

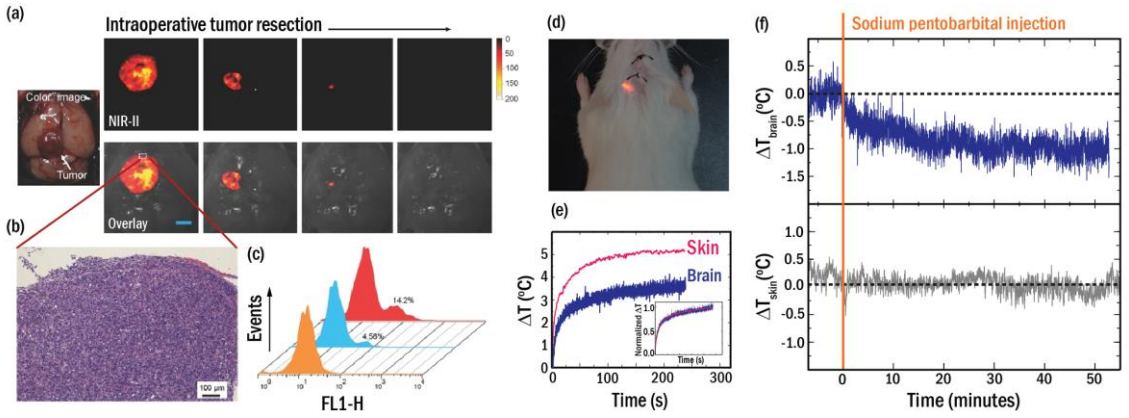

Figure 4. Ag_2S NPs for brain studies. (a) Step-by-step *in vivo* NIR-II-guided tumor resection using Gd-Ag_2S nanoprobes (top: NIR-II fluorescence images; bottom: overlay images of brightfield and NIR-II fluorescence). The scale bar corresponds to 2.5 mm. **(b)** Haemotoxylin and Eosin (H&E)-stained section of excised tumor tissue. **(c)** Histogram profiles of residual tumor cells obtained by flow cytometry for NIR-II-guided surgery (blue) and naked eye surgery (red). Reproduced with permission from reference 87. Copyright Wiley-VCH 2015. **(d)** NIR-II fluorescence (overlaid with bright field image) of intracerebrally injected Ag_2S NPs in a CD1 mouse. **(e)** Brain and skin surface temperature increase under laser-induced heating. **(f)** Change in brain and skin surface temperature during a barbiturate coma. Adapted with permission from reference 94. Copyright Wiley-VCH 2018.

IV.c.- Selectively-targeted imaging by Ag_2S NPs.

In vivo target delivering of NIR-II emitting NPs, whether just for specific imaging and diagnostics or for multifunctional theranostics, is a paradigm in the field of nanomedicine. Many studies for surface modification of such NPs are being conducted but successful examples are rather elusive. This might be due to the relative novelty of NIR-II whole-body imaging as well as to the difficulty in achieving good surface decoration. For the particular case of Ag_2S NPs, as recently reviewed by Lu *et al.*, specific targeting has been successfully achieved in a few cases.[95] In all of them, Ag_2S NPs were specifically functionalized for the *in vivo* detection of cancer tumors following different approaches that are summarized next:

i) The first one consists in the surface decoration of Ag_2S NPs with folic acid so that *in vivo* tumor detection is achieved by taking into account the overexpression of folate receptors in various cancer cells.[87, 96, 97]

ii) Tumor detection via its induced changes in local vasculature was achieved by decorating Ag_2S NPs surface with antibodies and peptides capable of selective attachment to vascular growth factors that are overexpressed in the angiogenesis associated with tumor development.[40]

iii) Localization and imaging of MCF 7 breast cancer cells with Ag_2S NPs was also achieved by surface decoration with DNA-aptamers. This approach was further improved in order to target the rare circulating tumor cells that are shed from tumors into the bloodstream by taking advantage of the synergy between Ag_2S and magnetic NPs.[51, 98]

iii) Bone metastasis was visualized *in vivo* using Ag_2S NPs surface-decorated with the approved drug alendronate, which is designed to target bones (specifically osteoclasts).[99] This is the first example of targeting *via* a small molecule drug and therefore of high importance for the future development of targeting with Ag_2S NPs.

iv) The most recent example of the use of Ag_2S NPs for in vivo detection of metastatic breast cancer cells was provided by Z. Wang *et al.*, who demonstrated selective adhesion of Ag_2S NPs to highly metastatic breast cancer cells (4T1 tumor model) via their CXC chemokine receptor 4 (CXCR4).[100] This was achieved through surface functionalization with a small molecule drug (plerixafor) for inhibition of CXCR4 and, hence, the use of the surface-decorated Ag_2S NPs (QD-AMD, see **Figure 5a** and **5b**) together with their photothermal properties resulted in a unique and tumor-specific theranostic element.

Although most of the works dealing with surface-decorated Ag_2S NPs were conducted with the ultimate objective of cancer imaging and diagnosis, it is important to acknowledge that imaging and diagnosis of cardiovascular diseases (CVDs) is gaining attention. CVDs are, indeed, the first cause of mortality in developed countries. Despite this increasing interest, there is only one work targeting Ag_2S NPs for the diagnosis and imaging of CVDs. Very recently, Ag_2S NPs were modified to endow them with adhesion to infarcted myocardial tissues. In particular, NIR-II imaging of infarcted hearts was demonstrated for the first time by employing Ag_2S NPs functionalized with angiotensin II (ATII), a short endogenous peptide that attaches to damaged myocardial cells due to the overexpression of the AT1R receptor.[101-103] D. Ortgies *et al.* demonstrated how Ag_2S-ATII NPs are capable of providing high contrast images of infarcted tissues in a rat's heart *ex vivo* (see **Figure 5c**). Furthermore, Ag_2S-ATII NPs made it possible to evaluate the different degrees of damage induced in the myocardium because of ischemia events of different durations. The results of this work revealed that the targeting efficiency and NIR-II fluorescence brightness of Ag_2S-ATII would allow their application in real-time, *in vivo* imaging and damage assessment of infarcted hearts via NIR-II luminescence. This could be a promising step towards the development of minimally invasive technologies for the infarct diagnosis at the preclinical level.

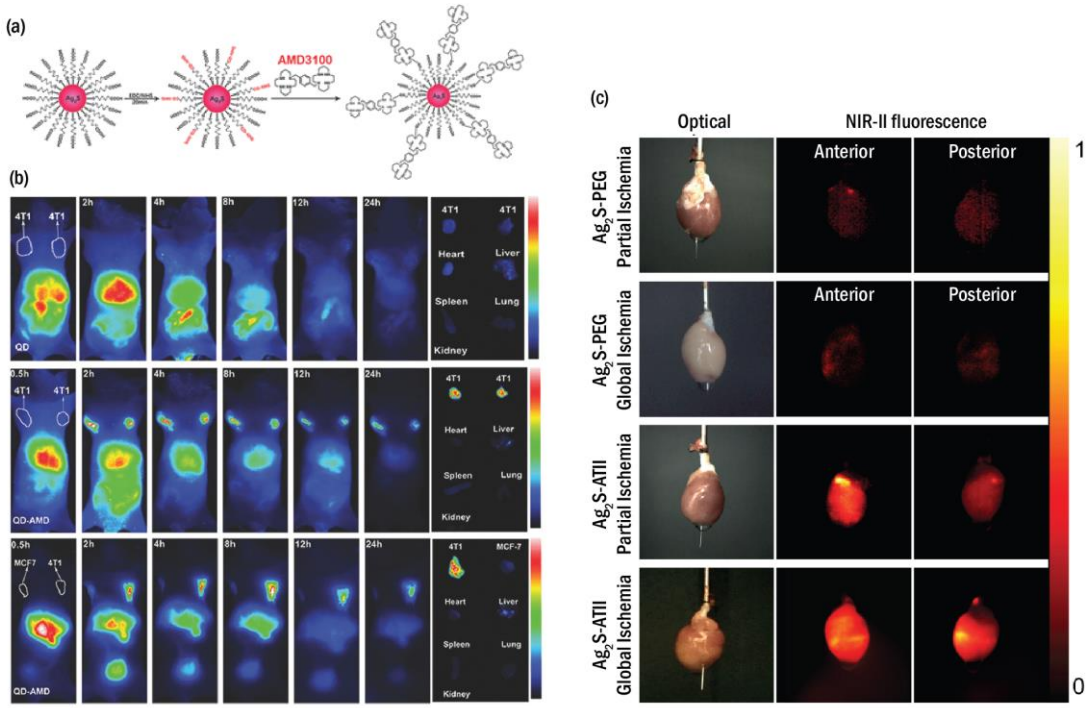

Figure 5. a) Schematic representation of Ag_2S NPs surface-functionalized with plerixaflor (QD- AMD). **b)** Top-row.- Time distribution in mice bearing bilateral 4T1 tumors employing non-targeting Ag_2S NPs and fluorescence of the excised organs, evidencing non selective accumulation. Middle row: *in vivo* imaging in mice bearing bilateral 4T1 tumors with QD- AMD showing accumulation in the tumors. Bottom row: *in vivo* imaging in mice bearing MCF- 7 and 4T1 tumors, respectively, at two axilla sites using QD- AMD resulting in selective marking of 4T1. **c)** Optical and fluorescence images of the infarcted (anterior) and the opposite (posterior) side of rat hearts exposed to 60 min partial and global ischemia. The non-specific Ag_2S-PEG NPs result only in weak fluorescence (top 2 rows), while the functionalized Ag_2S-ATII NPs demonstrate their targeting of infarcted tissues, illustrated by the partial ischemia (3rd row) where only one side of the heart is affected and the global event, where damaged tissue is identified on both sides (4th row). Adapted with permission from references 100 and 101. Copyright 2018 WILEY- VCH Verlag GmbH & Co. KGaA, Weinheim and Tsinghua University Press and Springer-Verlag GmbH Germany, part of Springer Nature 2019

IV.d- Other specific applications of Ag_2S NPs.

Shifting away from imaging, thermometry and photothermal therapy, a few recently published impactful showcases of the great potential of Ag_2S NPs in theranostic applications including cell tracking and multimodal tumor therapy will be highlighted in this section.

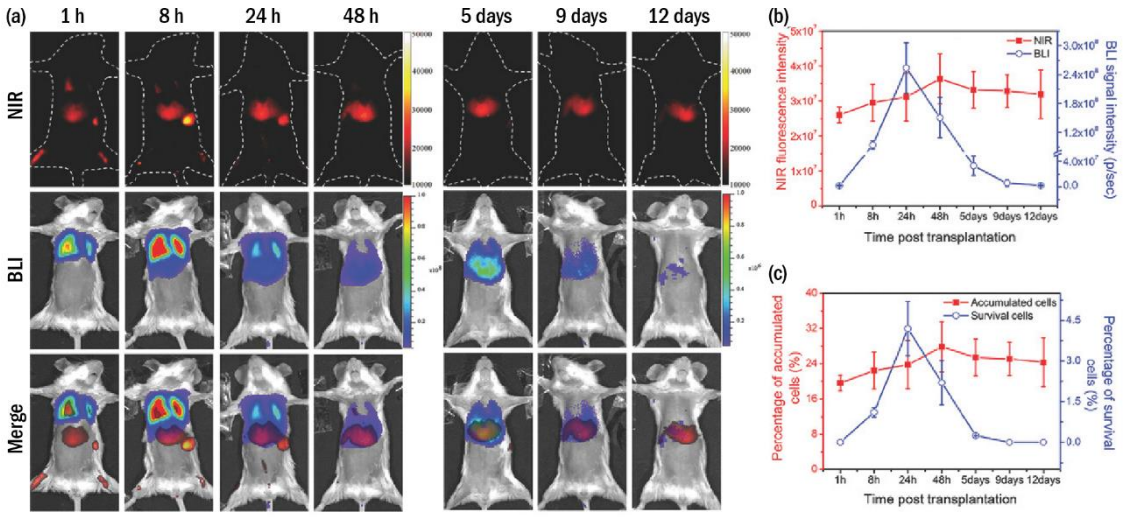

Figure 6. a) *In vivo* tracking of intravenously transplanted mMSCs for liver regeneration, NIR-II fluorescence images, BLI images, and merged images of mice with acute liver failure. **b)** Quantitative analyses of the cell accumulation and survival in liver by the total NIR fluorescence intensities of NIRFI and the total photon flux (photons s^{-1}) of BLI. **c)** Quantitative analyses of the accumulation and survival ratios of mMSCs in liver. Adapted with permission from reference 105. Copyright 2018, Wiley- VCH.

Stem-cell-based therapy is currently investigated as promising treatment for many diseases were new therapeutic approaches are urgently required, such as cardiac, neurological, and hepatic diseases.[104] However, the fate of stem cells after transplantation, including their distribution, viability, and cell clearance, is a kind of knowledge not yet obtained in a reliable way. Indeed, stem cells after transplantation experience a very different microenvironment from *in vitro*, and their viability *in vivo* is critical to the therapeutic effect. Therefore, it is essential to understand the process and the underlying mechanism of their regeneration for successful therapies. G. Chen *et al.* demonstrated how NIR-II fluorescence imaging can be used to dynamically monitor the distribution of labelled stem cells after transplantation in a mouse model.[105] In this case, Ag_2S NPs worked synergistically with the luciferase-based endogenous red bioluminescence (BLI). The former allowed locating to locate and quantifying the transplanted mouse mesenchymal stem cells (mMSCs) and the latter served to locate and quantify the viable mMSCs. The NIR-II emission of Ag_2S NPs enabled visualizing the whole-body distribution and translocation of living and death cells after intravenous transplantation (**Figure 6a**). That insight was unachievable by employing exclusively the BLI method or through recent MRI methods for cell death imaging. BLI alone only allows observing the living cells, while leaving the distribution and translocation of dead cells unresolved. At the same time, MRI fails to assess the survival or proliferation of stem cells after transplantation. The reliable quantitative tracking (**Figures 6b-c**) supplied through the Ag_2S-based approach also allowed the authors to improve the understanding on how stem

cells help liver regeneration, a step of paramount relevance for stem cells-based therapy.

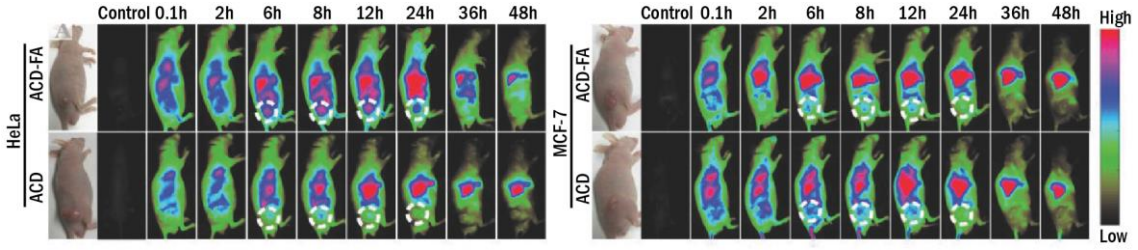

Figure 7. a) *In vivo* NIR fluorescence imaging and **b)** fluorescence intensity of different tumor-bearing mice after injection with different probes (ACD and ACD-FA, see main text), the white dotted circle was the tumor site, *p < 0.05, **p < 0.01, ***p < 0.001. Reproduced with permission from reference 106. Copyright Wiley-VCH, 2018.

In 2018, good example of synergetic theranostics was published by K. Cheng *et al*. The authors designed a multifunctional nanocluster probe (hereafter ACD) loaded with Ag_2S QDs, chlorin e6 (Ce6) chemotherapy drug (doxorubicin, DOX), and then linked it to DSPE-mPEG2000-folate (ACD-FA).[106] Then, a synergy of photodynamic, chemo- and photothermal therapies against the tumor was provided by the different materials constituting the nanocluster. Its three-component therapeutic effect was better than single- or two component treatment. Authors explained how by monitoring the biodistribution of the probe in the whole body and tumor microvessels of mice (**Figure 7a-b**), the different components (chemotherapy, PTT, and controlled PDT) of the combined treatment could be accurately guided. The photodynamic "switching" effect of the probe enabled by Ag_2S significantly increased the specific photodynamic effect of Ce6, and the DOX-responsive release effect observably reduced the tumor-specific release of DOX. The comparative improvement in respect to alternative therapies also stemmed from a reduction in the nonspecific toxicity of the probe, while enhancing the specific therapeutic effect and minimizing the injected dose effectively.

Finally the work published by K. Cheng *et al.* should be highlighted as authors demonstrate for the first time the potential use of Ag_2S NPs as photodynamic (PDT) agents for *in vivo* tumor cell suppression using NIR light irradiation.[107] The as-synthesized (high temperature pyrolysis) Ag_2S NPs were modified with polyethylene glycol (PEGylated) phospholipids. In such a configuration, the NPs could trigger singlet oxygen ($^1O_2$) production. Based on this, the authors demonstrated selective irreversible damage of tumor cells under 808 nm laser irradiation. Furthermore, polydopamine (PDA) was coupled to the surface of the Ag_2S NPs, bestowing the Ag_2S-PDA NPs with more intense PDT effects. This enhancement was explained in terms of the large reactive oxygen singlet production achieved through the regulation of PDA. As a remarkable output of this work, the superior capability of longer-wavelength excitation light to penetrate

deeper into tissues suggest the potential development of *in vivo* PDT by using Ag_2S NPs as photosensitizers

Besides the three recent reports discussed above, Ag_2S NPs have also been used for other innovative applications. including molecular imaging ,[108-111] NIR-II tracked drug loading,[112] NIR-II/photoacoustic-monitored photothermal therapy,[41] and NIR-II biosensing combined with photothermal therapy.[113] For a more detailed account of those reports, see the aforementioned review paper by Lu *et al.*.[95]

V.- Conclusions: limitations, challenges and perspectives.

Placing the above described results in the context of the state of the art in NIR-II bioimaging, Ag_2S NPs are likely to play a crucial role in the near future in bringing multimodal NIR-II imaging and self-monitored photothermal therapy closer to the clinics. Nevertheless, such translation of Ag_2S into the clinics would require to overcome some limitations. These, together with the work required to address them, are listed next:

i) Brightness: the NIR-II fluorescence brightness of Ag_2S NPs is nowadays limited by their relative low QY, as discussed in section II. Generally speaking, Ag_2S NPs dispersed in water typically show QYs below 1%, likely due to the presence of surface defects. Improving the brightness requires removing these defects. This, in turn, calls for the development of new synthesis approaches that minimize the non-radiative decay probabilities. In our opinion, these new synthesis approaches should be based in the synergy between different routes, from pure chemical routes to better passivate the surface to post processing techniques such as ultrafast laser irradiation.

ii) Mass production: translation into clinics would require a large number of experiments. This, in turn, would require syntheses at a larger scale. Nowadays, commercial Ag_2S NPs are far from being inexpensive. As an average number, 1 mL of an aqueous dispersion of PEG-coated Ag_2S NPs costs 500 €. This price should be substantially reduced to enable all the trials required for their eventual clinical approval. It is necessary to explore new synthesis approaches capable of mass production of high quality Ag_2S NPs at reduced costs. Of course, the fabrication costs will depend on the market demand. It is necessary to convince the groups working on preclinical imaging of the advantages of Ag_2S NPs and this requires that forthcoming works move away from the proof-of-concept works seen up to this moment and start dealing with more specific and advanced bioapplications. The participation of clinicians at this stage would be essential.

iii) Toxicity, clearance and biodistribution: there are numerous works reporting on the low toxicity of Ag_2S NPs both *in vivo* and *in vitro*.[95, 114] In most cases, the toxicity has been evaluated in immortalized cell lines, such as cancer cells, or by monitoring basic parameters of animal models after systematic administration of Ag_2S NPs. It is needed, however, to expand these studies to non-immortalized cell lines. At the same time, more refined *in vivo* toxicity experiments are required by, for instance, using metabolic cages. At the same time, the biodistribution of Ag_2S NPs is still not fully understood, as it does not only depend on particle size and surface decoration but it also varies from batch to batch. This must be addressed before considering any clinical applications, as a full knowledge of biodistribution and clearance routes of any contrast agent or therapeutic drug is essential.

iv) Standardized characterization of thermo-optical properties: it has been evidenced that one of the most interesting property of Ag_2S NPs is their potential use as a multi-parametric nanothermometers. This, in turns would make possible non-invasive *in vivo* thermometry for disease diagnosis. This temperature sensing is accompanied by a non-negligible light-to-heat conversion efficiency, facilitating the development of NIR-II self-monitored photothermal therapy. This is, even at a preliminary research stage, a very rare and appreciated advantage and will be crucial in clinical translation. There is no rival for Ag_2S NPs at sight, in that regard. But before going further into the *in vivo* applications, a more careful characterization of Ag_2S NPs as luminescent nanothermometers is required. In particular, it is essential to report the thermal response of Ag_2S NPs in conditions equivalent to those found *in vivo*. This requires the definition, in accordance with the scientific community, of a set of standard conditions in which the thermal response of Ag_2S NPs should be measured. This will allow not only the full understanding of the *in vivo* thermal readouts provided by Ag_2S NPs but also a reliable comparison of their thermal sensitivities with other NIR-II fluorescent nanothermometers.

We are firmly convinced that overcoming the above listed limitations is feasible and that in a very near future, a new generation of Ag_2S NPs with improved properties will be available to the scientific community working on preclinical imaging and theranostics. It is difficult at this point to predict the possible appearance of other systems that beat the performance of Ag_2S NPs as multifunctional units. Even if Ag_2S NPs were eventually overcome by other systems, we are firmly convinced that for a long time they will be the top rival to beat. Indeed, the performance of the new NPs proposed as alternative to Ag_2S NPs (thermal sensitivity, brightness, spectral stability, etc.) will act as merit figures with which to compare their opponents.

ACKNOWLEDGMENTS

This work was supported by the Spanish Ministry of Economy and Competitiveness under projects MAT2016-75362-C3-1-R, MAT2017-83111R, and MAT2017-85617-R, by the Instituto de Salud Carlos III (PI16/00812), by the Comunidad Autónoma de Madrid (B2017/BMD-3867RENIMCM), and co-financed by the European Structural and investment fond. Additional funding was provided by the European Commission, Horizon 2020 project NanoTBTech, and also by COST action CM1403. D. H. O. is grateful to the Instituto de Salud Carlos III for a Sara Borrell scholarship (No. CD17/00210). D. R thanks IMDEA Nanoscience for his contract. A.B. thanks the European Commission as this project has received funding from the European Union's Horizon 2020 research and innovation program under the Marie Skłodowska Curie grant agreement no. 709270 TEMPTATION."

REFERENCES

1. Jaque, D.; Richard, C.; Viana, B.; Soga, K.; Liu, X.; Solé, J. G. *Advances in Optics and Photonics* **2016,** 8, (1), 1-103.
2. Alivisatos, A. P. *Science* **1996,** 271, (5251), 933-937.
3. Alivisatos, A. P.; Gu, W.; Larabell, C. *Annual Review of Biomedical Engineering* **2005,** 7, 55-76.
4. Bera, D.; Qian, L.; Tseng, T.-K.; Holloway, P. H. *Materials* **2010,** 3, (4), 2260-2345.
5. Maestro, L. M.; Haro-González, P.; Iglesias-de la Cruz, M. C.; SanzRodríguez, F.; Juarranz, Á.; Solé, J. G.; Jaque, D. *Nanomedicine* **2013,** 8, (3), 379-388.
6. Maestro, L. M.; Rodríguez, E. M. n.; Rodríguez, F. S.; la Cruz, M. l.-d.; Juarranz, A.; Naccache, R.; Vetrone, F.; Jaque, D.; Capobianco, J. A.; Solé, J. G. a. *Nano Lett.* **2010,** 10, (12), 5109-5115.
7. Yang, J.-M.; Yang, H.; Lin, L. *ACS Nano* **2011,** 5, (6), 5067-5071.
8. Dubertret, B.; Skourides, P.; Norris, D. J.; Noireaux, V.; Brivanlou, A. H.; Libchaber, A. *Science* **2002,** 298, (5599), 1759-1762.
9. Larson, D. R.; Zipfel, W. R.; Williams, R. M.; Clark, S. W.; Bruchez, M. P.; Wise, F. W.; Webb, W. W. *Science* **2003,** 300, (5624), 1434-1436.
10. Anderson, R. R.; Parrish, J. A. *J. Invest. Dermatol.* **1981,** 77, (1), 13-9.
11. Troy, T. L.; Thennadil, S. N. *J. Biomed. Opt.* **2001,** 6, (2), 167-176.
12. Bashkatov, A.; Genina, E.; Kochubey, V.; Tuchin, V. *J. Phys. D: Appl. Phys.* **2005,** 38, (15), 2543.
13. Smith, A. M.; Mancini, M. C.; Nie, S. *Nat. Nanotechnol.* **2009,** 4, 710-711.
14. Benayas, A.; Ren, F.; Carrasco, E.; Marzal, V.; del Rosal, B.; Gonfa, B. A.; Juarranz, Á.; Sanz-Rodríguez, F.; Jaque, D.; García-Solé, J. *Adv. Funct. Mater.* **2015,** 25, (42), 6650-6659.
15. Imamura, Y.; Yamada, S.; Tsuboi, S.; Nakane, Y.; Tsukasaki, Y.; Komatsuzaki, A.; Jin, T. *Molecules* **2016,** 21, (8), 1080.
16. Ren, F.; del Rosal, B.; An, S. Y.; Yang, F.; Carrasco, E.; Benayas, A.; Oh, J. K.; Jaque, D.; de la Fuente, Á. J.; Vetrone, F. *Particle & Particle Systems Characterization* **2017,** 34, (2), 1600242.
17. Funke, K. *Science and Technology of Advanced Materials* **2013,** 14, (4), 043502.
18. Huxter, V. M.; Mirkovic, T.; Nair, P. S.; Scholes, G. D. *Adv. Mater.* **2008,** 20, (12), 2439-2443.
19. Kashida, S.; Watanabe, N.; Hasegawa, T.; Iida, H.; Mori, M.; Savrasov, S. *Solid State Ionics* **2003,** 158, (1), 167-175.
20. Mansour, A.; Razafinimanana, M.; Monthioux, M.; Pacheco, M.; Gleizes, A. *Carbon* **2007,** 45, (8), 1651-1661.
21. Eatemadi, A.; Daraee, H.; Karimkhanloo, H.; Kouhi, M.; Zarghami, N.; Akbarzadeh, A.; Abasi, M.; Hanifehpour, Y.; Joo, S. W. *Nanoscale Res Lett* **2014,** 9, (1), 393-393.
22. Wang, Z.; Gu, T.; Kadohira, T.; Tada, T.; Watanabe, S. *The Journal of Chemical Physics* **2008,** 128, (1), 014704.
23. He, H.; Lin, Y.; Tian, Z.-Q.; Zhu, D.-L.; Zhang, Z.-L.; Pang, D.-W. *Small* **2018,** 14, (11), 1703296.
24. Akamatsu, K.; Takei, S.; Mizuhata, M.; Kajinami, A.; Deki, S.; Takeoka, S.; Fujii, M.; Hayashi, S.; Yamamoto, K. *Thin Solid Films* **2000,** 359, (1), 55-60.
25. Brühwiler, D.; Leiggener, C.; Glaus, S.; Calzaferri, G. *The Journal of Physical Chemistry B* **2002,** 106, (15), 3770-3777.
26. Xu, C.; Zhang, Z.; Ye, Q. *Materials Letters* **2004,** 58, (11), 1671-1676.
27. Schaaff, T. G.; Rodinone, A. J. *The Journal of Physical Chemistry B* **2003,** 107, (38), 10416-10422.

28. Zheng, M.; Li, Y.; Liu, S.; Wang, W.; Xie, Z.; Jing, X. *ACS Applied Materials & Interfaces* **2016,** 8, (36), 23533-23541.
29. Cui, C.; Li, X.; Liu, J.; Hou, Y.; Zhao, Y.; Zhong, G. *Nanoscale Res Lett* **2015,** 10, (1), 431.
30. Zhang, Y.; Liu, Y.; Li, C.; Chen, X.; Wang, Q. *The Journal of Physical Chemistry C* **2014,** 118, (9), 4918-4923.
31. Lin, S.; Feng, Y.; Wen, X.; Zhang, P.; Woo, S.; Shrestha, S.; Conibeer, G.; Huang, S. *The Journal of Physical Chemistry C* **2015,** 119, (1), 867-872.
32. Ruiz, D.; Mizrahi, M.; Santos, H. D. A.; Jaque, D.; Jones, C. M. S.; Marqués-Hueso, J.; Jacinto, C.; Requejo, F. G.; Torres-Pardo, A.; González-Calbet, J. M.; Juárez, B. H. *Nanoscale* **2019,** 11, (18), 9194-9200.
33. Doh, H.; Hwang, S.; Kim, S. *Chem. Mater.* **2016,** 28, (22), 8123-8127.
34. Wang, Y.; Li, X.; Xu, M.; Wang, K.; Zhu, H.; Zhao, W.; Yan, J.; Zhang, Z. *Nanoscale* **2018,** 10, (5), 2577-2587.
35. Hocaoglu, I.; Demir, F.; Birer, O.; Kiraz, A.; Sevrin, C.; Grandfils, C.; Yagci Acar, H. *Nanoscale* **2014,** 6, (20), 11921-11931.
36. Du, Y.; Xu, B.; Fu, T.; Cai, M.; Li, F.; Zhang, Y.; Wang, Q. *J. Am. Chem. Soc.* **2010,** 132, (5), 1470-1471.
37. Wu, P.-J.; Yu, J.-W.; Chao, H.-J.; Chang, J.-Y. *Chem. Mater.* **2014,** 26, (11), 3485-3494.
38. Jiang, P.; Tian, Z.-Q.; Zhu, C.-N.; Zhang, Z.-L.; Pang, D.-W. *Chem. Mater.* **2012,** 24, (1), 3-5.
39. Jiang, P.; Zhu, C.-N.; Zhang, Z.-L.; Tian, Z.-Q.; Pang, D.-W. *Biomaterials* **2012,** 33, (20), 5130-5135.
40. Wang, Y.; Yan, X.-P. *Chemical Communications* **2013,** 49, (32), 3324-3326.
41. Yang, T.; Tang, Y. a.; Liu, L.; Lv, X.; Wang, Q.; Ke, H.; Deng, Y.; Yang, H.; Yang, X.; Liu, G.; Zhao, Y.; Chen, H. *ACS Nano* **2017,** 11, (2), 1848-1857.
42. Kong, L.; Liu, W.; Chu, X.; Yao, Y.; Zhu, P.; Ling, X. *RSC Adv.* **2015,** 5, (98), 80530-80535.
43. Wang, C.; Wang, Y.; Xu, L.; Zhang, D.; Liu, M.; Li, X.; Sun, H.; Lin, Q.; Yang, B. *Small* **2012,** 8, (20), 3137-3142.
44. Gui, R.; Wan, A.; Liu, X.; Yuan, W.; Jin, H. *Nanoscale* **2014,** 6, (10), 5467-5473.
45. He, H.; Lin, Y.; Tian, Z. Q.; Zhu, D. L.; Zhang, Z. L.; Pang, D. W. *Small* **2018,** 14, (11), 1703296.
46. Zhang, H.; Hyun, B.-R.; Wise, F. W.; Robinson, R. D. *Nano Letters* **2012,** 12, (11), 5856-5860.
47. Jiang, P.; Zhu, D.-L.; Zhu, C.-N.; Zhang, Z.-L.; Zhang, G.-J.; Pang, D.-W. *Nanoscale* **2015,** 7, (45), 19310-19316.
48. Song, J.; Ma, C.; Zhang, W.; Li, X.; Zhang, W.; Wu, R.; Cheng, X.; Ali, A.; Yang, M.; Zhu, L.; Xia, R.; Xu, X. *ACS Applied Materials & Interfaces* **2016,** 8, (37), 24826-24836.
49. Yang, H.-Y.; Zhao, Y.-W.; Zhang, Z.-Y.; Xiong, H.-M.; Yu, S.-N. *Nanotechnology* **2013,** 24, (5), 055706.
50. Öberg, V. A.; Zhang, X.; Johansson, M. B.; Johansson, E. M. J. *ChemNanoMat* **2018,** 4, (12), 1223-1230.
51. Gao, J.; Wu, C.; Deng, D.; Wu, P.; Cai, C. *Advanced Healthcare Materials* **2016,** 5, (18), 2437-2449.
52. Tan, L.; Wan, A.; Li, H. *Langmuir* **2013,** 29, (48), 15032-15042.
53. Asik, D.; Yagci, M. B.; Demir Duman, F.; Yagci Acar, H. *Journal of Materials Chemistry B* **2016,** 4, (11), 1941-1950.
54. Ruiz, D.; del Rosal, B.; Acebrón, M.; Palencia, C.; Sun, C.; Cabanillas-González, J.; López-Haro, M.; Hungría, A. B.; Jaque, D.; Juarez, B. H. *Adv. Funct. Mater.* **2017,** 27, (6), 1604629.
55. Ding, C.; Cao, X.; Zhang, C.; He, T.; Hua, N.; Xian, Y. *Nanoscale* **2017,** 9, (37), 14031-14038.

56. Zhang, Y.; Zhao, N.; Qin, Y.; Wu, F.; Xu, Z.; Lan, T.; Cheng, Z.; Zhao, P.; Liu, H. *Nanoscale* **2018,** 10, (35), 16581-16590.
57. Zhang, Y.; Hong, G.; Zhang, Y.; Chen, G.; Li, F.; Dai, H.; Wang, Q. *ACS Nano* **2012,** 6, (5), 3695-702.
58. Bhavane, R.; Starosolski, Z.; Stupin, I.; Ghaghada, K. B.; Annapragada, A. *Scientific Reports* **2018,** 8, (1), 14455.
59. Rocha, U.; Kumar, K. U.; Jacinto, C.; Villa, I.; Sanz-Rodríguez, F.; del Carmen Iglesias de la Cruz, M.; Juarranz, A.; Carrasco, E.; van Veggel, F. C. J. M.; Bovero, E.; Solé, J. G.; Jaque, D. *Small* **2014,** 10, (6), 1141-1154.
60. Villa, I.; Vedda, A.; Cantarelli, I.; Pedroni, M.; Piccinelli, F.; Bettinelli, M.; Speghini, A.; Quintanilla, M.; Vetrone, F.; Rocha, U.; Jacinto, C.; Carrasco, E.; Rodríguez, F.; Juarranz, Á.; del Rosal, B.; Ortgies, D.; Gonzalez, P.; Solé, J.; García, D. *Nano Res.* **2015,** 8, (2), 649-665.
61. Naczynski, D. J.; Tan, M. C.; Zevon, M.; Wall, B.; Kohl, J.; Kulesa, A.; Chen, S.; Roth, C. M.; Riman, R. E.; Moghe, P. V. *Nat. Commun.* **2013,** 4, 2199-2199.
62. Welsher, K.; Sherlock, S. P.; Dai, H. *Proc Natl Acad Sci U S A* **2011,** 108, (22), 8943-8.
63. Jaque, D.; Vetrone, F. *Nanoscale* **2012,** 4, (15), 4301-4326.
64. Ximendes, E. C.; Santos, W. Q.; Rocha, U.; Kagola, U. K.; Sanz-Rodríguez, F.; Fernández, N.; Gouveia-Neto, A. d. S.; Bravo, D.; Domingo, A. M.; del Rosal, B.; Brites, C. D. S.; Carlos, L. D.; Jaque, D.; Jacinto, C. *Nano Lett.* **2016,** 16, (3), 1695-1703.
65. Brites, C. D. S.; Lima, P. P.; Silva, N. J. O.; Millan, A.; Amaral, V. S.; Palacio, F.; Carlos, L. D. *Nanoscale* **2012,** 4, (16), 4799-4829.
66. Brites, C. D.; Lima, P. P.; Silva, N. J.; Millán, A.; Amaral, V. S.; Palacio, F.; Carlos, L. D. *Adv. Mater.* **2010,** 22, (40), 4499-4504.
67. Balabhadra, S.; Debasu, M. L.; Brites, C. D.; Nunes, L. A.; Malta, O. L.; Rocha, J.; Bettinelli, M.; Carlos, L. D. *Nanoscale* **2015,** 7, (41), 17261-17267.
68. Santos, H.; Ruiz, D.; Lifante, G.; Jacinto, C.; Juarez, B.; Jaque, D. *Nanoscale* **2017,** 9, (7), 2505-2513.
69. Okabe, K.; Inada, N.; Gota, C.; Harada, Y.; Funatsu, T.; Uchiyama, S. *Nat. Commun.* **2012,** 3, 705.
70. Olkhovets, A.; Hsu, R. C.; Lipovskii, A.; Wise, F. W. *Phys. Rev. Lett.* **1998,** 81, (16), 3539-3542.
71. Jaque Garcia, D.; Garcia Sole, J., Quantum Dot Fluorescence Thermometry. In *Thermometry at the Nanoscale: Techniques and Selected Applications*, The Royal Society of Chemistry: 2016; pp 83-123.
72. Balabhadra, S.; Debasu, M. L.; Brites, C. D. S.; Ferreira, R. A. S.; Carlos, L. D. *The Journal of Physical Chemistry C* **2017,** 121, (25), 13962-13968.
73. Botas, A. M. P.; Brites, C. D. S.; Wu, J.; Kortshagen, U.; Pereira, R. N.; Carlos, L. D.; Ferreira, R. A. S. *Particle & Particle Systems Characterization* **2016,** 33, (10), 740-748.
74. Carrasco, E.; del Rosal, B.; Sanz-Rodríguez, F.; de la Fuente, Á. J.; Gonzalez, P. H.; Rocha, U.; Kumar, K. U.; Jacinto, C.; Solé, J. G.; Jaque, D. *Adv. Funct. Mater.* **2015,** 25, (4), 615-626.
75. Balabhadra, S.; Debasu, M. L.; Brites, C. D. S.; Rocha, J.; Carlos, L. D. *J. Lumin.* **2016,** 180, 25-30.
76. Zhao, D.-H.; Yang, J.; Xia, R.-X.; Yao, M.-H.; Jin, R.-M.; Zhao, Y.-D.; Liu, B. *Chemical Communications* **2018,** 54, (5), 527-530.
77. del Rosal, B.; Carrasco, E.; Ren, F.; Benayas, A.; Vetrone, F.; Sanz-Rodríguez, F.; Ma, D.; Juarranz, Á.; Jaque, D. *Adv. Funct. Mater.* **2016,** 26, (33), 6060-6068.
78. Zhu, X.; Feng, W.; Chang, J.; Tan, Y.-W.; Li, J.; Chen, M.; Sun, Y.; Li, F. *Nat. Commun.* **2016,** 7, 10437.
79. Wissler, E. H. *Journal of Applied Physiology* **1998,** 85, (1), 35-41.
80. Pennes, H. H. *Journal of Applied Physiology* **1948,** 1, (2), 93-122.

81. Diller, K. R.; Ryan, T. P. *Journal of Heat Transfer* **1998,** 120, (4), 810-829.
82. Ximendes, E. C.; Rocha, U.; Sales, T. O.; Fernández, N.; Sanz-Rodríguez, F.; Martín, I. R.; Jacinto, C.; Jaque, D. *Adv. Funct. Mater.* **2017,** 27, (38), 1702249.
83. Ximendes, E. C.; Rocha, U.; del Rosal, B.; Vaquero, A.; Sanz-Rodríguez, F.; Monge, L.; Ren, F.; Vetrone, F.; Ma, D.; García-Solé, J. *Advanced healthcare materials* **2017,** 6, (4), 1601195.
84. Santos, H. D. A.; Ximendes, E. C.; Iglesias-de la Cruz, M. d. C.; Chaves-Coira, I.; del Rosal, B.; Jacinto, C.; Monge, L.; Rubia-Rodríguez, I.; Ortega, D.; Mateos, S.; GarcíaSolé, J.; Jaque, D.; Fernández, N. *Advanced Functional Materials* **2018,** 28, (43), 1803924.
85. Dong, X. *Theranostics* **2018,** 8, (6), 1481-1493.
86. Wang, H.; Mu, X.; Yang, J.; Liang, Y.; Zhang, X.-D.; Ming, D. *Coordination Chemistry Reviews* **2019,** 380, 550-571.
87. Li, C.; Cao, L.; Zhang, Y.; Yi, P.; Wang, M.; Tan, B.; Deng, Z.; Wu, D.; Wang, Q. *Small* **2015,** 11, (35), 4517-4525.
88. Kiyatkin, E. A.; Brown, P. L. *Physiology & behavior* **2005,** 84, (4), 563-570.
89. Bejanian, M.; Jones, B. L.; Syapin, P. J.; Finn, D. A.; Alkana, R. L. *Pharmacology Biochemistry and Behavior* **1991,** 39, (2), 457-463.
90. Wang, H.; Wang, B.; Normoyle, K. P.; Jackson, K.; Spitler, K.; Sharrock, M. F.; Miller, C. M.; Best, C.; Llano, D.; Du, R. *Frontiers in neuroscience* **2014,** 8, 307.
91. Bola, R. A.; Kiyatkin, E. A. *Neuropharmacology* **2017,** 126, 271-280.
92. Kiyatkin, E. A.; Brown, P. L.; Wise, R. A. *European Journal of Neuroscience* **2002,** 16, (1), 164-168.
93. Ward, T. R.; Svensgaard, D. J.; Spiegel, R. J.; Puckett, E. T.; Long, M. D.; Kinn, J. B. *Bioelectromagnetics* **1986,** 7, (3), 243-258.
94. del Rosal, B.; Ruiz, D.; Chaves-Coira, I.; Juárez, B. H.; Monge, L.; Hong, G.; Fernández, N.; Jaque, D. *Advanced Functional Materials* **2018,** 28, (52), 1806088.
95. Chenghao, L.; Guihuan, C.; Bing, Y.; Hailin, C. *Adv. Eng. Mater.* **2018,** 0, (0), 1700940.
96. Zhang, R. Y.; Wang, Z. Y.; Yang, X. Q.; Xuan, Y.; Cheng, K.; Li, C.; Song, X. L.; An, J.; Hou, X. L.; Zhao, Y. D. *Nanotechnology* **2018,** 29, (5).
97. Song, Y.-Y.; Li, C.; Yang, X.-Q.; An, J.; Cheng, K.; Xuan, Y.; Shi, X.-M.; Gao, M.-J.; Song, X.-L.; Zhao, Y.-D.; Chen, W. *Journal of Materials Chemistry B* **2018,** 6, (29), 4808-4820.
98. Ding, C.; Zhang, C.; Yin, X.; Cao, X.; Cai, M.; Xian, Y. *Analytical Chemistry* **2018,** 90, (11), 6702-6709.
99. Li, C.; Zhang, Y.; Chen, G.; Hu, F.; Zhao, K.; Wang, Q. *Advanced Materials* **2017,** 29, (13), 1605754.
100. Wang, Z.; Ma, Y.; Yu, X.; Niu, Q.; Han, Z.; Wang, H.; Li, T.; Fu, D.; Achilefu, S.; Qian, Z.; Gu, Y. *Advanced Functional Materials* **2018,** 28, (23), 1800732.
101. Ortgies, D. H.; García-Villalón, Á. L.; Granado, M.; Amor, S.; Rodríguez, E. M.; Santos, H. D. A.; Yao, J.; Rubio-Retama, J.; Jaque, D. *Nano Res.* **2019,** 12, (4), 749-757.
102. Dvir, T.; Bauer, M.; Schroeder, A.; Tsui, J. H.; Anderson, D. G.; Langer, R.; Liao, R.; Kohane, D. S. *Nano Lett.* **2011,** 11, (10), 4411-4414.
103. Hu, J.; Ortgies, D. H.; Martín Rodríguez, E.; Rivero, F.; Aguilar Torres, R.; Alfonso, F.; Fernández, N.; Carreño-Tarragona, G.; Monge, L.; Sanz-Rodriguez, F.; Iglesias, M. d. C.; Granado, M.; García-Villalon, A. L.; García Solé, J.; Jaque, D. *Advanced Optical Materials* **2018,** 6, (22), 1800626.
104. Trounson, A.; DeWitt, N. D. *Nature Reviews Molecular Cell Biology* **2016,** 17, 194.
105. Chen, G.; Lin, S.; Huang, D.; Zhang, Y.; Li, C.; Wang, M.; Wang, Q. *Small* **2018,** 14, (3), 1702679.

106. Cheng, K.; Yang, X.-Q.; Zhang, X.-S.; Chen, J.; An, J.; Song, Y.-Y.; Li, C.; Xuan, Y.; Zhang, R.-Y.; Yang, C.-H.; Song, X.-L.; Zhao, Y.-D.; Liu, B. *Advanced Functional Materials* **2018,** 28, (36), 1803118.
107. Cheng, K.; Zhang, X.-S.; An, J.; Li, C.; Zhang, R.-Y.; Ye, R.; Ye, B.-J.; Liu, B.; Zhao, Y.-D. *Chemistry – A European Journal* **2019,** 25, (31), 7553-7560.
108. Tan, L.; Huang, R.; Li, X.; Liu, S.; Shen, Y.-M.; Shao, Z. *Carbohydrate Polymers* **2017,** 157, 325-334.
109. Wu, F.-F.; Zhou, Y.; Wang, J.-X.; Zhuo, Y.; Yuan, R.; Chai, Y.-Q. *Sensors and Actuators B: Chemical* **2017,** 243, 1067-1074.
110. Yan, D.; He, Y.; Ge, Y.; Song, G. *Sensors and Actuators B: Chemical* **2017,** 240, 863-869.
111. Jin, H.; Gui, R.; Gong, J.; Huang, W. *Biosensors and Bioelectronics* **2017,** 92, 378-384.
112. Song, C.; Zhang, Y.; Li, C.; Chen, G.; Kang, X.; Wang, Q. *Advanced Functional Materials* **2016,** 26, (23), 4192-4200.
113. Li, S.; Xu, L. G.; Sun, M. Z.; Wu, X. L.; Liu, L. Q.; Kuang, H.; Xu, C. L. *Adv. Mater.* **2017,** 29, (19), 1606086.
114. Zhang, Y.; Zhang, Y.; Hong, G.; He, W.; Zhou, K.; Yang, K.; Li, F.; Chen, G.; Liu, Z.; Dai, H.; Wang, Q. *Biomaterials* **2013,** 34, (14), 3639-3646.